Aalto University

OPEN ACCESS

This is an electronic reprint of the original article.
This reprint may differ from the original in pagination and typographic detail.

Sourroubille, Marie; Miranda-Valdez, Isaac Y.; Mäkinen, Tero; Koivisto, Juha; Alava, Mikko J.

Thermogelation of methylcellulose

Published in:
Colloids and Surfaces A: Physicochemical and Engineering Aspects

DOI:
10.1016/j.colsurfa.2024.136057

Published: 20/03/2025

Document Version
Publisher's PDF, also known as Version of record

Published under the following license:
CC BY

Please cite the original version:
Sourroubille, M., Miranda-Valdez, I. Y., Mäkinen, T., Koivisto, J., & Alava, M. J. (2025). Thermogelation of methylcellulose: A rheological approach with Gaussian Process Regression. *Colloids and Surfaces A: Physicochemical and Engineering Aspects*, *709*, Article 136057. https://doi.org/10.1016/j.colsurfa.2024.136057

This material is protected by copyright and other intellectual property rights, and duplication or sale of all or part of any of the repository collections is not permitted, except that material may be duplicated by you for your research use or educational purposes in electronic or print form. You must obtain permission for any other use. Electronic or print copies may not be offered, whether for sale or otherwise to anyone who is not an authorised user.

Colloids and Surfaces A: Physicochemical and Engineering Aspects 709 (2025) 136057

Contents lists available at ScienceDirect

Colloids and Surfaces A: Physicochemical and Engineering Aspects

journal homepage: www.elsevier.com/locate/colsurfa

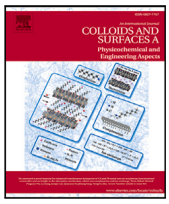

Thermogelation of methylcellulose: A rheological approach with Gaussian Process Regression

Marie Sourroubille, Isaac Y. Miranda-Valdez *, Tero Mäkinen, Juha Koivisto, Mikko J. Alava

Complex Systems and Materials, Department of Applied Physics, Aalto University, P.O. Box 11000, Espoo, FI-00076 Aalto, Finland

GRAPHICAL ABSTRACT

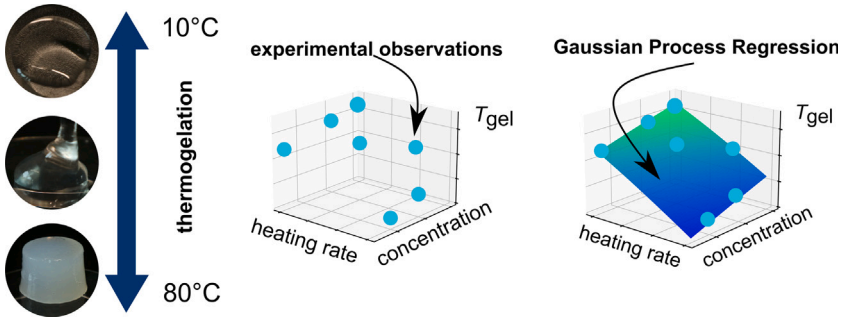

ARTICLE INFO

Keywords:
Gaussian Process Regression
Rheology
Hydrogel
Methylcellulose
Active learning

ABSTRACT

The rheological characterization of thermoresponsive polymers typically demands extensive experimental observations across multiple parameters. The present work demonstrates how Gaussian Process Regression (GPR) can expedite this process by efficiently characterizing the thermogelation of methylcellulose fluids. By employing GPR as a surrogate model for Active Learning, we capture the effects of multiple parameters on the gelation dynamics of methylcellulose, requiring fewer experimental observations than traditional factorial design experiments. Additionally, we leverage the common rheological practice of frequency sweep analysis at step-increasing temperatures using GPR. Our work shows how GPR models can be trained to predict rheological behaviors at both short and long timescales, and even to predict rheological material functions. These findings suggest that GPR is a powerful tool for enhancing the efficiency and depth of rheological characterization, making it highly valuable for both research and industrial applications.

1. Introduction

The digital revolution of the 21st century features Machine Learning (ML) as a tool for translating data into knowledge. By exploiting techniques such as clustering, principal component analysis, and Gaussian processes (GPs), the use of ML has permeated many fields. Remarkably, ML has changed how natural sciences abstract from observations to build and test hypotheses. This is extensively observed in materials science research, where ML enhances and integrates the synthesis, characterization, and modeling of materials [1–6]. ML in material science has paved a different way to establish structure–property relationships.

ML applied to material science eases establishing structure–property relationships, thus steering material discovery. For example, neural networks have provided highly accurate predictions of stable crystal structures; simultaneously, they reduced the workload for scientists [7–9]. Nevertheless, despite all the spanning applications of neural

* Corresponding author.
E-mail address: isaac.mirandavaldez@aalto.fi (I.Y. Miranda-Valdez).

https://doi.org/10.1016/j.colsurfa.2024.136057
Received 29 April 2024; Received in revised form 20 December 2024; Accepted 25 December 2024
Available online 7 January 2025
0927-7757/© 2025 The Authors. Published by Elsevier B.V. This is an open access article under the CC BY license (http://creativecommons.org/licenses/by/4.0/).

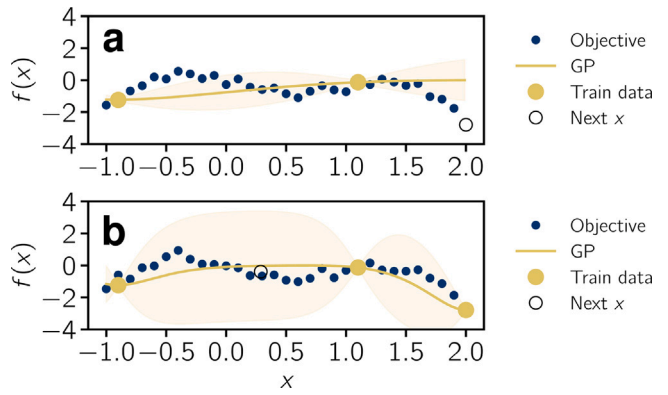

Fig. 1. Example of Active Learning for predicting an expensive function $f(x)$. a Two initial data points fitted with a Gaussian process compared to the unknown objective function. Computing the acquisition function (here expected improvement) and finding its maximum suggests the location of the next measurement point to the user. b Iterating the process a second time shows how the prediction has improved compared to the unknown objective. One can continue to iterate until a given condition is satisfied.

networks in materials research, they work based on large datasets. Therefore, they have limited use in experimental research. The reality is that experimental data acquisition can be challenging due to its expensive and time-consuming nature, often forcing scientists to deal with small datasets [10].

How can ML be incorporated when working with small datasets in materials research? A less-used method is Gaussian Process Regression (GPR). Recently, GPR has gathered attention since it solves one of the typical conditions for ML; it does not need large amounts of data. Furthermore, GPR can be used to implement Bayesian Optimization (BO), which in material science serves as a probabilistic design of experiment framework [11–14]. BO is a method based on Bayes' theorem; one assumes prior knowledge exists to estimate a posterior solution. Therefore, BO combined with GPR can actively guide robust simulations and hands-on experiments toward exploring or exploiting areas of interest [13,14]. The latter is possible with decision-making algorithms where a model is first trained using GPR and then improved using new data in a process called Active Learning (AL) [13].

Active Learning involves two steps that Fig. 1a,b exemplifies: predicting the variable of interest that maximizes or minimizes a material property and making a decision based on that prediction [15–18]. The first step in the ML process is to fit a portion of the dataset to a surrogate function, typically a Gaussian process [11,19]. The second step involves selecting the next sampling point through an acquisition or utility function. The acquisition function balances exploration and exploitation in areas of high uncertainty and potential for "good" performance [11,12,14].

Integrating the surrogate and acquisition functions into an algorithm has demonstrated significant value in materials research. For instance, Ziatdinov et al. [20] have shown that AL can automate real-time data acquisition with scanning probe microscopy. The ML algorithm created a high-throughput workflow where prior knowledge determined the next sampling location for the microscope probe. Similarly, Pedersen et al. [21] and Torsti et al. [6] used AL to generate a workflow for simulating high-entropy alloys. From an initial set of compositions, AL guided in real-time what compositions to simulate next based on prior knowledge and by looking for the alloy with the highest current density or mechanical strength, respectively. All these are examples of AL guiding materials research, minimizing the workload and computation time.

In the first part of this article, we used BO to guide the rheological characterization of methylcellulose (MC) aqueous systems. While BO has been used in simulations and high-throughput AL workflows, its effectiveness in hands-on experiments is yet to be fully proven [20–22]. Using BO is of great interest as it could reduce experimental workload in rheometry; one needs to characterize materials by varying experimental parameters. Accordingly, here we showcase how BO allows for the gelation temperature of MC to be characterized across varying conditions. We chose to study MC – a biopolymer that undergoes thermally-induced gelation (thermogelation) – as it is an important food additive and precursor material for sustainable packaging [23–25]. Comprehending how thermogelation phenomena change with varying experimental conditions is crucial to improve these applications. On the other hand, the second part of this article presents GPR as a valuable tool for exploiting rheological data and understanding the rheological behavior of MC. We hypothesize that GPR can accelerate the rheological characterization of thermoresponsive MC solutions and allow us to characterize the effect of frequency (ω) and temperature (T) on their thermogelation, a process without time–temperature superposition.

Overall, we evaluated the rheological properties of MC aqueous systems as a function of varying the polymer concentration, heating kinetics, and angular frequency. Using rheometry and ML, we characterized the gelation temperature (T_{gel}) of the MC system at varying conditions. Then, from two T_{gel} points characterized under different circumstances, we fitted the data to a GP and computed the acquisition function to identify the next "good" sampling point. According to this next sampling point, we prepared the MC system with the suggested polymer concentration and characterized the T_{gel} at the suggested heating rate. Then, we used GPR as a regression tool for assessing the effect of angular frequency and temperature on the rheological properties of MC.

2. Experimental methods

2.1. Materials

This research used a food-grade methylcellulose labeled Benecel™ MX MC-50000 from Ashland Specialties Belgium. As per the provider, MC-50000 indicates a viscosity of approximately 50 Pa s for a 2 wt.% aqueous solution. Structural and chemical data for the MC used here has been reported elsewhere [24]. In brief, the MC has an average molecular weight of 534 kg mol^{-1}, degree of substitution (DS) of 1.87, and intrinsic viscosity [η] at 25 °C of 1351 ml g^{-1}. Suspensions were prepared by dispersing such MC in deionized ultrapure Milli-Q water at 60 °C, after which the suspensions were tempered at 3 °C for 12 h before characterization. The solid fraction of MC in each suspension varied between 1.0 and 2.3 wt.%. This concentration range (c) is interesting for manufacturing cellulose foams and formulating food [23,25–27]. In some MC suspensions, cellulose fibers, Kraft lignin, or graphite were used as rheology modifiers. The cellulose fibers were bleached softwood kraft pulp from CMPC (Chile) [28]. Kraft lignin, BioPiva™ 100, was purchased from UPM Biochemicals (Finland) [29]. Synthetic graphite powder with particle size <20 μm was bought from Sigma-Aldrich (USA).

2.2. Rheometry

Rheological characterization was carried out with an Anton Paar (Austria) modular compact rheometer 302 equipped with a wide-gap Couette geometry [30]. The rheological setup involves a cup (CC27, Anton Paar) at the bottom and a tool with ridged walls on top (CC17, Anton Paar). The MC suspension was carefully poured into the cup without creating any bubbles to conduct the tests. Next, the tool was moved down to its measuring position. Before starting the experiment, the sample was left to settle for around 20 min at a temperature of 10 °C to guarantee the restoration of its structure.

2.2.1. Dynamic mechanical thermal analysis

We used dynamic mechanical thermal analysis (DMTA) for AL. DMTA is an isochronous experiment and consists of applying a sinu-

soidal strain (ε) with amplitude ε_0,

$$\varepsilon(\omega,t) = \varepsilon_0 \sin(\omega t), \tag{1}$$

where t is the time, and ω is the angular frequency. For AL, the rheological properties of MC were assessed within the linear viscoelastic region by applying a $\varepsilon_0 = 0.5\%$ at $\omega = 10$ rad s^{-1}. In such cases, the rheological properties depend on the temperature (T), which changes at a constant rate during the experiment. The experiments started from 10 °C and went to 80 °C with a constant heating rate ranging from 0.5 to 2 °C min^{-1}. The maximum temperature was defined by experimenting with different temperature intervals (e.g., 10–40 °C, 10–45 °C, and so forth).

For measuring the viscoelastic response, it is assumed that $\varepsilon(\omega,t)$ produces a shear stress signal $\tau(\omega,t)$ with two components, one in-phase with the imposed strain and one in-phase with the imposed strain rate, described by

$$\tau(\omega,t) = \tau_0 \sin(\omega t)\cos(\delta) + \tau_0 \cos(\omega t)\sin(\delta), \tag{2}$$

where τ_0 is the shear stress amplitude, and δ is the phase shift angle between the stress and strain waves. From Eq. (2), one can separate the shear stress signal in two components known as storage modulus (G') and loss modulus (G''); the first one describes the elastic behavior and the second the viscous behavior. Alternatively, using complex notation, the material function is given by the complex shear modulus (G^*). In DMTA, the material functions were recorded as a function of T, as

$$G'(\omega,T) = \frac{\tau_0}{\varepsilon_0}\cos(\delta), \tag{3}$$

and

$$G''(\omega,T) = \frac{\tau_0}{\varepsilon_0}\sin(\delta). \tag{4}$$

Methylcellulose exhibits a thermogelation transition. Such transition temperature (T_{gel}) is critical for many manufacturing processes where MC is a crucial constituent. T_{gel} can be computed from the phase shift angle (δ) measured from DMTA, defined as

$$\delta = \arctan\frac{G''(\omega,T)}{G'(\omega,T)}. \tag{5}$$

Recalling that δ is a parameter that defines the viscoelastic nature of a system, a drastic change in δ denotes a change in its configuration ($0 < \delta < \pi/2$). Therefore, the method to extract T_{gel} is described in Fig. S1a,b. Fig. S1a shows the typical behavior of $G'(\omega,T)$ and $G''(\omega,T)$, while Fig. S1b depicts the behavior of δ as a function of T. From Fig. S1b, T_{gel} is computed as the point where the linear function fitting the damping plateau intercepts the polynomial function fitting the exponential decay [19,24–26,30].

2.2.2. Dynamic mechanical analysis

Performing DMTA with ω different than 10 rad s^{-1} led to unsuccessful experiments due to non optimal combinations of heating rate, data acquisition, and ω. Accordingly, to assess the effect of ω on the thermogelation of MC, we performed dynamic mechanical analysis (DMA). Eqs. (1)–(5) apply to DMA as well since DMA is an isothermal version of DMTA, evaluating G' and G'' as a function of ω. DMA used $\varepsilon_0 = 0.5\%$ and 0.01 rad s^{-1} < ω < 100 rad s^{-1}. From the experiments, we characterized the storage $G'(\omega,T)$ and loss $G''(\omega,T)$ modulus functions at 10 °C, 20 °C, …, 80 °C and 70 °C, 60 °C, …, 10 °C (the protocol lasted 24 h, and the mass loss was less than 0.9%).

2.3. Active learning and Gaussian process regression

The first part of the results of this paper is about AL. We assessed the effect of two parameters, heating rate and MC concentration, on the T_{gel} by guiding the experimental process with a ML algorithm. The algorithm works based on Bayesian Optimization [19]. The surrogate function of the algorithm is a Gaussian Process Regressor ($GPR_{T_{gel}}$) with a radial basis function (RBF) kernel implemented in Scikit-learn [31]. Furthermore, we used expected improvement (EI) as the acquisition function. Algorithm 1 describes the pseudocode of the AL process.

Algorithm 1 Pseudocode for Active Learning

1: Load initial rheology training data D_1
2: For $n = 1, 2, \ldots$, do
3: Optimize length scale for training data
4: Fit the Gaussian Process Regressor $f(x; D_n)$
5: Active learning: choose the next sampling point $x_{n+1} = \text{argmax}\,\text{EI}(x)$
6: New experiment to obtain y_{n+1}
7: Augment data $D_{n+1} = \{D_n, (x_{n+1}, y_{n+1})\}$
8: End for.

To start the AL process, we determined the T_{gel} from two random experiments within the boundaries of the parameters. We used these two data points as training data for the GPR. Then, the acquisition function suggested where to measure next in a loop until the standard deviation (σ) levels off, reaching the measuring resolution of the rheometer.

For the second part of this paper, we used $GPR_{G',G''}$ (same implementation as described for AL) to create an ML model with the DMA data. The reader can find more information about the ML implementation in the supplementary material.

3. Results and discussion

To familiarize the reader with the thermogelation phenomena of MC aqueous systems, we first describe the behavior of $G'(\omega,T)$ and $G''(\omega,T)$ during DMTA. Fig. 2a–h depicts $G'(\omega,T)$ during heating and cooling within various temperature intervals. Fig. 2h details the typical behavior of $G'(\omega,T)$ for MC aqueous systems, similar to the one reported in the literature for MC and other thermo-responsive systems [32,33]. Specifically, it indicates that the storage modulus slightly decreased from 10 to 50 °C. This process led to a rapid increase in $G'(\omega,T)$, which leveled off at 80 °C. The sharp rise of $G'(\omega,T)$ after 50 °C implies a change in consistency from a viscoelastic liquid to a viscoelastic solid. The rheological behavior characterized in Fig. 2h agrees with experimental observations for similar methylcellulose systems [34]. This change happened as MC chains percolated into a fibril network during a self-assembly process [35–37]. During the cooling process, there was a significant hysteresis shown by $G'(\omega,T)$ as the fibril network dissolved [38,39]. As for $G''(\omega,T)$, Fig. 2i shows that it followed the same trend as $G'(\omega,T)$ but the increment after reaching a temperature of 50 °C was less remarkable. In the end, $G''(\omega,T)$ depicted a butterfly-looking hysteresis loop, representing the formation (heating) and dissolution (cooling) of a metastable phase [24].

In the literature, the material functions $G'(\omega,T)$ and $G''(\omega,T)$ are systematically evaluated for MC as in Fig. 2h; this is, within a defined temperature interval typically ranging from 20 to 80 °C [35,40–42]. The reason for evaluating this interval is intuitive; it probes the whole thermogelation phenomena in MC. However, what happens when the thermogelation process is interrupted is less researched. Therefore, in Fig. 2, we evaluated $G'(\omega,T)$ and $G''(\omega,T)$ within different temperature intervals, thereby observing how the thermogelation hysteresis changed as a function of the maximum heating temperature. For the MC system evaluated in Fig. 2h, we estimated a T_{gel} of 51.83 °C. In Fig. 2a, one can observe that when the maximum temperature was below T_{gel}, the hysteresis in $G'(\omega,T)$ and $G''(\omega,T)$ was almost neglectable. On the contrary, Fig. 2b–h shows an increasing hysteresis effect when heating above T_{gel}.

In Fig. 2b, the hysteresis appeared when the maximum heating temperature was 51 °C. This suggests the formation and dissolution of a premature fibril structure. As the maximum temperature was increased in subsequent Fig. 2c–g, the storage modulus hysteresis evolved until taking on its well-known shape in Fig. 2h. Hysteresis was already present when heating to 51 °C, which coincided with the estimated

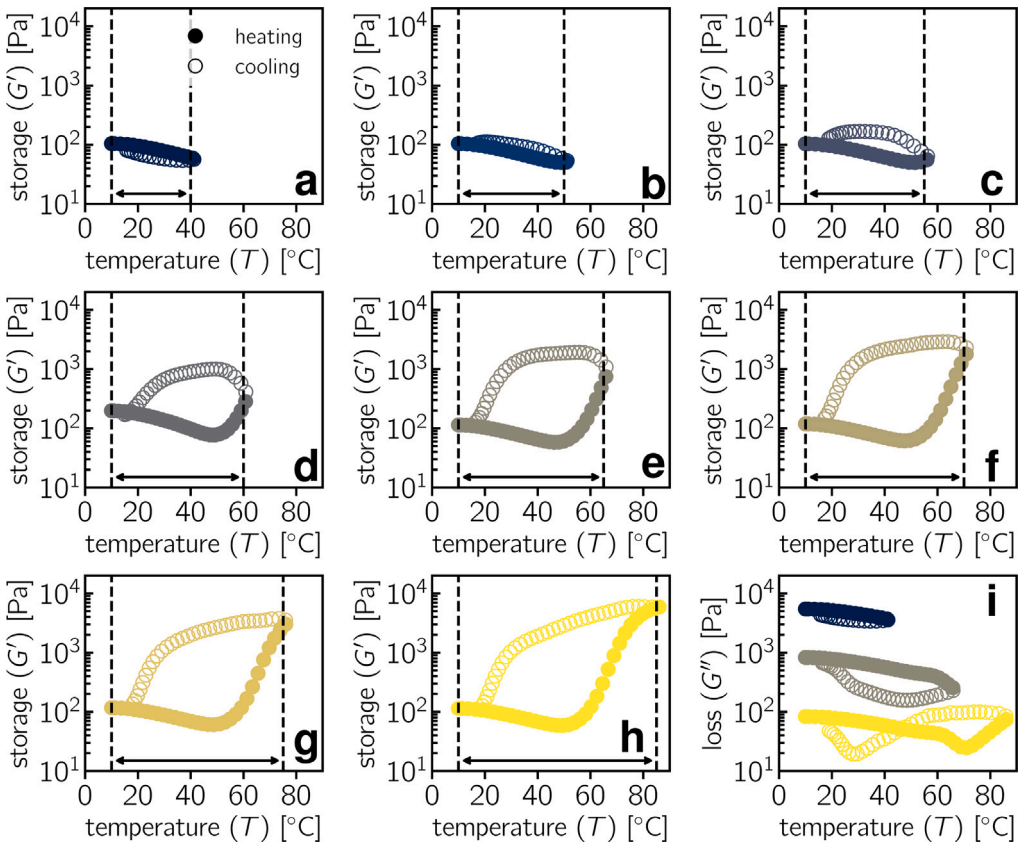

Fig. 2. Dynamic mechanical thermal analysis: effect of the maximum heating temperature on the hysteresis loop shape of storage (G') and loss modulus (G'') of a MC suspension with 2 wt.% concentration (c) for a given constant angular frequency ($\omega = 10$ rad s^{-1}) and temperature ramp (2 °C min^{-1}). a–h G' hysteresis as a function of temperature (T). i G'' hysteresis as a function of T (G'' values are shifted for the sake of visualization; the plots overlap without shifting them).

$T_{gel} = 51.83$ °C of MC. This indicates that the method of calculating T_{gel} from $\delta(\omega, T)$ is an approximation of when the fibril formation process begins.

By observing the evolution of $G''(\omega, T)$ as the temperature interval widens (Fig. 2i), the butterfly-looking hysteresis only appeared when the MC system was heated to $T \geq 80$ °C. This butterfly indicates that the test captured all the steps involved in the thermogelation phenomena for MC. Accordingly, the DMTA experiments were designed to convey the temperature range from 10 to 80 °C for the AL process.

3.1. Active learning of DMTA experiments

Characterizing the gelation temperature (T_{gel}) as a function of multiple parameters is crucial for developing applications for MC systems. For instance, knowing the T_{gel} of MC during the production of cellulose foams is essential for estimating the energy cost of the drying process. On the other hand, in food systems, T_{gel} can determine the consistency of food [30,43]. This study evaluated two parameters, namely heating rate and MC concentration, significantly influencing T_{gel} [32]. Although it is well known that T_{gel} changes as a function of concentration and heating kinetics, to our knowledge, no work in the literature evaluates the effect of these two parameters together. To fill this research gap, we used a ML algorithm based on BO and AL, as described in the experimental methods. We must remark that we attempted to include the effect of varying ω, but this led to unsuccessful DMTA experiments due to measuring limitations when combining, for example, low frequencies with fast heating rates. To observe the effect of ω, we performed DMA; these DMA results are discussed in the next section with $GPR_{G',G''}$.

In Fig. 3a–i, the AL sequence for mapping T_{gel} as a function of heating rate and concentration is shown. The sequence began in Fig. 3a–c (first iteration), where two aleatory T_{gel} were characterized within the parameter space. The surface in Fig. 3a represents the mean value μ of the GP obtained by fitting these two initial data points to the surrogate function. However, this fitting had high standard deviation values σ in regions far from the data points, as observed in Fig. 3b. EI was computed to obtain the next sampling location as shown in Fig. 3c. Since σ was high for the first iteration, we adjusted the additional contribution parameter $\xi = 0.1$ °C to exploit the highly uncertain areas. As a result, the suggested sampling location is determined to be at argmax EI.

In the second iteration (Fig. 3d–f), we fitted the surrogate function to the T_{gel} dataset once again, but this time augmented with the result obtained at the location suggested from the first iteration. Fig. 3e shows that adding a third T_{gel} data point reduced significantly the standard deviation of the GP fitting compared to σ in Fig. 3b. However, despite the reduction, the new σ was still considerably large. Therefore, we recomputed the acquisition function to obtain the next sampling location. We fixed again ξ to 0.1 °C to exploit the high uncertainty area and obtain the next sampling location near argmax EI.

In Fig. 3g–i, the results of the third iteration are presented. What stands out from this iteration is that σ began to level off (Fig. 3h), while the GP surface (Fig. 3g) did not show significant improvements. Such observations indicated that the acquisition function needed to be changed to favor the exploration of the parameter space. Accordingly, the acquisition function was computed using $\xi = 2$ °C. Otherwise, the maximum of the EI would have continued to suggest measuring close to the region with the lowest σ and highest μ, that is, around the same sampling point indicated from the second iteration.

In total, we performed six iterations, and from seven data points, we built the surface in Fig. 4a, which contains the $GPR_{T_{gel}}$ prediction within the parameter space boundaries. One can compare the seven data points of the AL framework to the 10 required by a two-level

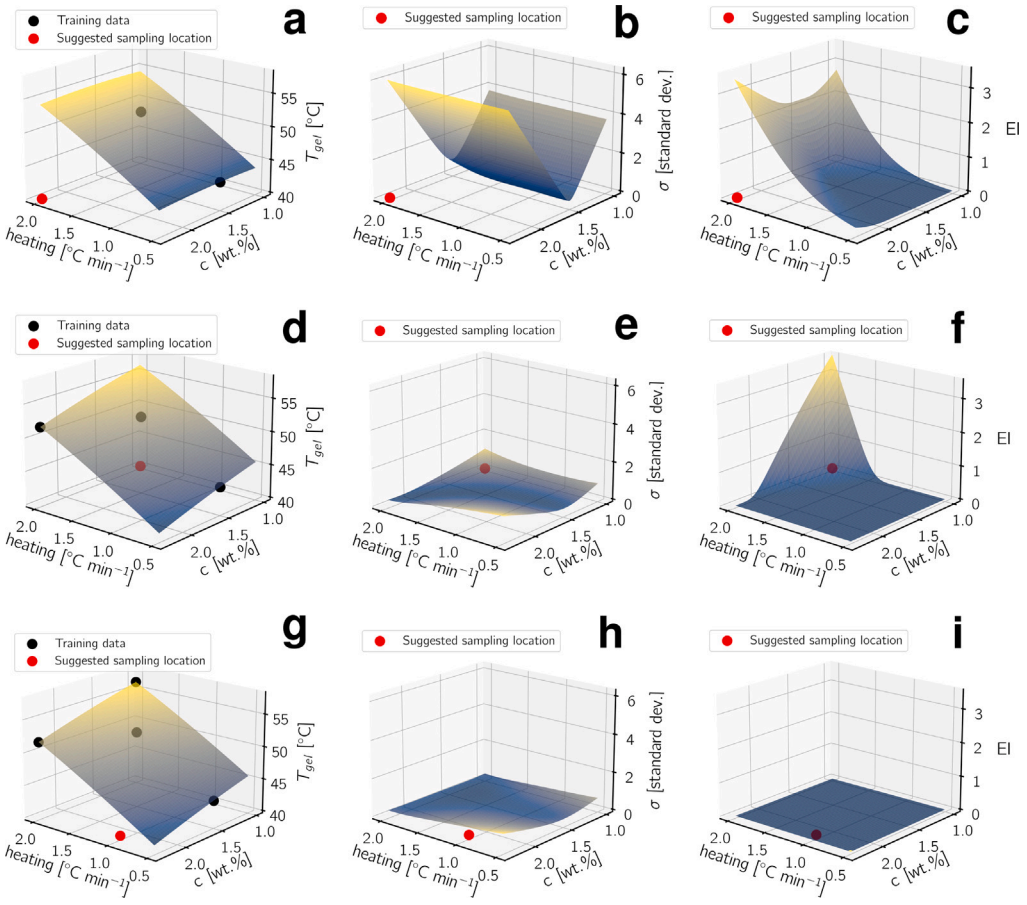

Fig. 3. Active Learning sequence to characterize the gelation temperature (T_{gel}) of MC as a function of heating rate and concentration using Bayesian Optimization with Gaussian process regressor as a surrogate function and expected improvement as an acquisition function. a–c First iteration showing the surrogate function prediction (a), standard deviation of the prediction (b), and EI computed to determine the next measuring point (c). d–f and g–i show the second and third iterations, respectively.

face-centered factorial design of experiments. After the final iteration, the σ surface in Fig. 4b leveled off to low values in the range of the experimental error. We assessed the robustness of the GPR$_{T_{gel}}$ prediction by adding test data points in Fig. 4a. To elaborate on the significance of Fig. 4a,b, Fig. 5a illustrates the variation of σ_{max} during each iteration. The point at which σ_{max} began to level off coincided with the iteration where we began to prioritize parameter space exploration. Ultimately, σ_{max} decreased to 0.48 °C. Fig. 5b demonstrates a strong agreement between the test data and the GPR$_{T_{gel}}$ prediction. Although the test data varied slightly from the prediction, the deviation was within the range of σ_{max}. In conclusion, AL successfully guided experimental research, as the surrogate function generated accurate predictions.

The final results from AL showed that increasing the concentration in the MC systems led to reducing T_{gel}, whereas fast heating rates favored an increment in T_{gel}. In previous research, Miranda-Valdez et al. [24] discussed the similarities between the T_{gel} of MC systems and the glass transition in polymers during oscillatory tests. Fig. 5c shows that when increasing the heating rate, MC macromolecules had a shorter time to respond to the mechanical stimulus during each oscillation; thus, T_{gel} presented thermal lag [38]. The glass transition of polymers exhibits the same thermal lag when characterized at high heating rates [44]. Contrarily, slow heating rates favored lower T_{gel} because MC macromolecules had more time to respond to the mechanical and thermal stimuli. One can observe in Fig. 5c that T_{gel} showed a 10 °C difference when characterized at 0.5 °C min^{-1} and 2.0 °C min^{-1} (constant concentration).

The effect of concentration on T_{gel} was the opposite of the heating rate. Increasing the concentration gave a lower T_{gel}. This occurred because the thermogelation of MC is a percolation phenomenon; therefore, a higher MC concentration favored the connectivity among the volume-spanning clusters, resulting in the fibril network formation process [30,39,45]. Fig. 5c depicts that T_{gel} slightly changed more with the concentration at slow heating rates. For example, at 0.5 °C min^{-1}, the T_{gel} for the systems with 1.0 wt.% concentration occurred at ~47 °C, whereas for the 2.3 wt.% concentration system T_{gel} was ~39 °C. On the other hand, at 2.0 °C min^{-1}, the systems with 1.0 and 2.3 wt.% had a T_{gel} of ~57 °C and ~51 °C, respectively.

One now may ask for different methods to affect the T_{gel} of MC. To assess that, we evaluated the effect of three additives on the T_{gel}. First, in Fig. S2a,b, we present the effect of cellulose fibers on $G'(\omega, T)$ and $G''(\omega, T)$. Adding cellulose fibers to MC systems with 1.5 wt.% concentration increased the magnitude of the material functions. Furthermore, increasing the fiber content decreased the T_{gel}, as shown in Fig. S2g. Cellulose fibers favored the connectivity in the MC systems, possibly due to the similar structure of cellulose and MC which favor the hydrophobic effect that induces the percolation [32]. The T_{gel} of MC has been shown to decrease when interacting with other polymers. For example, adding polyethylene glycol to MC systems has also significantly reduced T_{gel} [26]. Evaluating the effect of cellulose fibers on the T_{gel} of MC is of great interest for manufacturing cellulose foams, where these two constituents are mixed to fabricate biodegradable replacements for plastics [23,46].

Another additive that is typically mixed with MC is lignin. Lignin is the second most abundant biopolymer on Earth; in recent years the biopolymer has been thoroughly researched, looking for new applications. One of these applications is to enhance the hydrophobicity of biobased polymers that could potentially replace plastics [25,47,48].

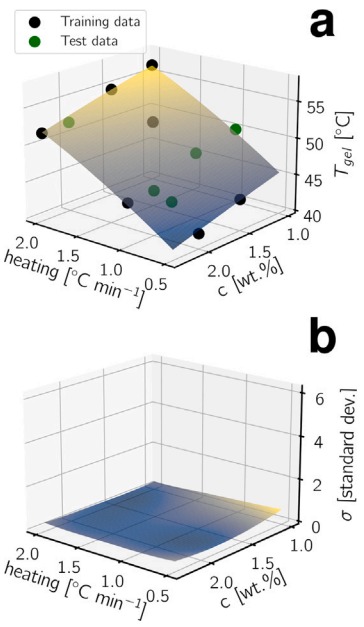

Fig. 4. Final result of the Active Learning sequence. a Prediction mean (μ) surface of the gelation temperature (T_{gel}) as a function of the heating rate and MC concentration. The μ surface is computed using the training data; test data is plotted to show the robustness of the prediction. b Standard deviation (σ) surface of the Gaussian process fitting the training data.

Therefore, we evaluated how adding Kraft lignin to MC systems affects T_{gel}. Fig. S2g shows that lignin enhanced the connectivity of MC since T_{gel} decreased by 3 °C. However, its effect on T_{gel} is less remarkable than adding cellulose fibers, which at large concentrations reduced T_{gel} by 10 °C.

We prepared suspensions with an "inert" additive (graphite) to understand better the interactions between MC dissolved in water and additives during gelation. The gelation temperature of the suspensions with graphite was investigated and compared with the corresponding suspensions that had cellulose fibers and lignin added individually, as shown in Fig. S2 g. Interestingly, increasing the graphite content had a small effect on T_{gel}, contrast to the effect observed when using cellulose fibers (Fig. S2 g), despite the graphite content being the same as the MC content. In the MC system, graphite remained "inert". Therefore, we can conclude that the interactions between MC and additives with similar chemical structures in suspension affect the gelation of MC aqueous systems.

To deepen the analysis, we assessed the T_{gel} of twenty suspensions containing different solid content of cellulose fibers, lignin, and graphite mixed in an MC system with a concentration of 1.5 wt.%. In this set of twenty samples, we randomly varied the content of cellulose fibers, lignin, and graphite in an MC system with fixed concentration. Each additive was varied in a range between 0.0 and 1.5 wt.%. Table S1 details the composition of each sample and its experimental T_{gel}. The results of T_{gel} were processed using GPR, and the contour plots in Fig. S3a–c were obtained using the GPR; such results demonstrate the application of GPR to analyze four-dimensional data. Fig. S3a–c shows the interaction of the three additives and their effect on the T_{gel} of MC. The contour plots show that the most significant contribution to enhancing the connectivity of MC came from the cellulose fiber content. Conversely, lignin reduced T_{gel} at concentrations lower than ~1.0 wt.%, whereas graphite could remain basically "inert" when its concentration did not exceed ~0.5 wt.%. Higher concentrations of graphite, as Fig. S3c depicts, lessened the interaction between lignin, cellulose fibers, and MC since only cellulose fibers contributed to a decrease in T_{gel}.

3.2. Gaussian process regression of DMA experiments

For the DMTA experiments, it was unfeasible to collect data while simultaneously changing both the heating rate and ω. Therefore, to examine the impact of ω on MC systems, we conducted DMA experiments and varied ω from 0.01 to 100 rad s^{-1}. We used three inputs (ω, T, and c) and two outputs (G' and G'') as the $GPR_{G',G''}$ training data. The $GPR_{G',G''}$ implementation from Scikit-learn allows multiple-output regression [21]. We rescaled the dataset before training the ML model to get the most accurate estimation of the covariance function length scale l. When dealing with rheological data gathered in the frequency or time spectrum, one can take advantage of the logarithmic nature of $G'(\omega)$ and $G''(\omega)$ to standardize the dataset scale. Accordingly, the GP was trained using $\log_{10}(\omega)$, $\log_{10}(G'')$, and $\log_{10}(G'')$. From herein, we refer to $\log_{10}$ when showing log; we remark on this since other ML implementations in the literature scale rheological functions using the natural logarithm (e.g., [4]). To make sure the scale of the feature T is consistent with the standardized training data, we divided it by a factor of 10.

Fig. 6 summarizes the performance of the $GPR_{G',G''}$. Fig. 6a,b corresponds to the trained model for heating, while Fig. 6d,e contains information about the performance with the cooling data. Both the heating and cooling models had a coefficient of determination R^2 = 0.991 for the features $\log(G')$ and $\log(G'')$, thus implying that the $GPR_{G',G''}$ can model the rheological data of MC. Fig. S4i,l shows that the model for heating and cooling had $l = 2.3$ and $l = 2.2$, respectively (in the units corresponding to the rescaled data). The length scale of the kernel is associated with the RBF covariance function and defines the smoothness and flexibility of the GP model. In the RBF kernel, l controls the "width" of the correlation between input points. A smaller length scale results in a more wiggly and flexible GP, allowing the function to vary more rapidly between points. On the other hand, a larger length scale results in a smoother GP, with a more gradual change between points. In both GP models, l is considerably large, considering the standardized scale of the training dataset, thus resulting in a smooth GP function.

Intuitively, one would define a length scale per input feature (i.e., $\log(\omega)$, $T \times 10^{-1}$, c). We did the latter in Fig. 6c,f, and the reader can compare the $GPR_{G',G''}$ performance with one or three length scales in Fig. S4. From Fig. 6c, one can analyze the length scales in the context of the original scale of each training dimension and use them as rheological descriptors of the system during heating and cooling. In heating, dimension 1 (ω) has a length scale of 3.72 decades in frequency; it implies that the material functions are strongly correlated over almost all the studied frequency range from 10^{-2} to 10^{2} rad s^{-1}. This strong correlation in frequency can be seen from Fig. S5, where $\log(G')$ and $\log(G'')$ depict a power-law behavior over almost four decades in frequency. Knowing that the material functions are strongly correlated over four decades supports findings in the literature that described the rheology of MC using a power-law [24].

The analysis for dimension 2 ($T \times 10^{-1}$) in Fig. 6c is more complex. However, one could assume that the length scale of 20.6 °C is correlated to the behaviors observed in the material functions when T increases. In other words, there are strongly correlated events every 20.6 °C. Upon increasing T, material functions initially decrease, then exponentially increase, and they finally depict a plateau. Finally, dimension 3 (c) has a length scale of 2.28 wt.%. As dimension 3 goes from 1 to 2 wt.%, the length scale indicates a strong correlation of the material functions over the concentration regime. This supports that material functions for MC gels increase as a power-law as a function of c. Indeed, for this system, material functions scale with c given an average power-law exponent of 3.95. Our findings suggest that using the length scales as rheological descriptors could open future venues for automating the selection of rheological models to fit the material functions. For instance, from the length scale in frequency, one can quickly choose a power-law model such as Scott-Blair's to fit $G'(\omega)$ and

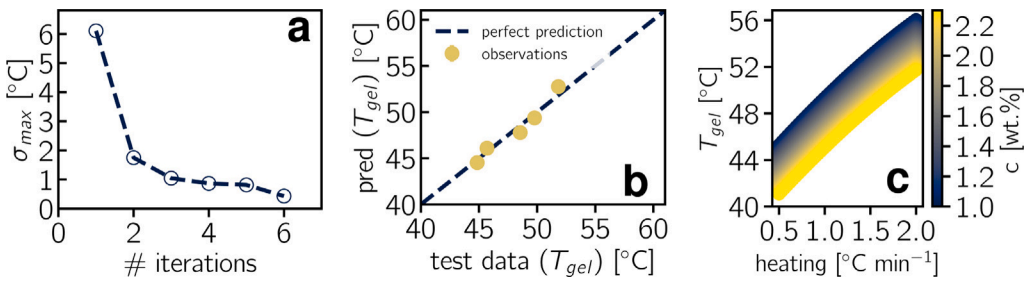

Fig. 5. Details of the Active Learning sequence and final results. a Evolution of the maximum standard deviation σ_{max} during each Active Learning iteration. b Surrogate function prediction compared to test data points (observations). c Surrogate function computed using the training data.

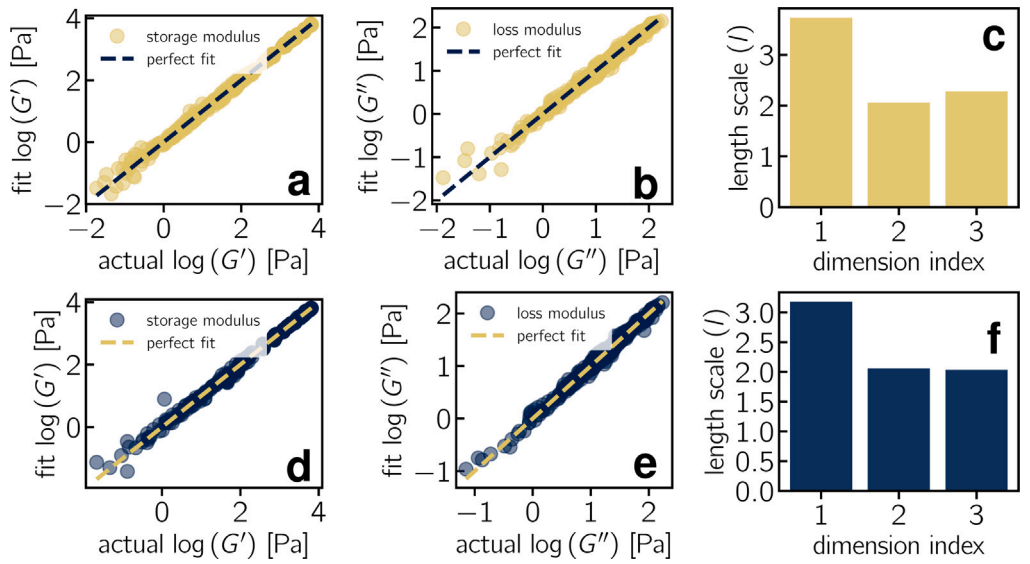

Fig. 6. Performance and length scales (l) of Gaussian Process model for heating and cooling of MC systems. The training data is isotropic dataset with angular frequency $\log(\omega)$ (dimension 1), temperature as $T \times 10^{-1}$ (dimension 2), and concentration c (dimension 3). a–c Performance of the GP model trained using $\log(\omega)$, $T \times 10^{-1}$, c as training space and storage $\log(G')$ and loss modulus $\log(G'')$ as target responses during the heating cycle of MC systems. d–f Performance of the GP model trained using $\log(\omega)$, $T \times 10^{-1}$, c as training space and storage $\log(G')$ and loss modulus $\log(G'')$ as target responses during the cooling cycle of MC systems.

$G''(\omega)$ [24].

Using the trained model, one can rescale the training features to their original form and construct hysteresis plots similar to those obtained from DMTA, as shown in Fig. 7a–o. In Fig. S5, the reader can find a 3D representation of the data in Fig. 7. The results Fig. 7a–o present $G'(T)$ and $G''(T)$ at angular frequencies that were not possible to measure physically. However, it is important to note that the effect of heating rate on the material functions of MC is complex but can be approximated to a very slow heating rate as the heating and cooling cycles lasted 24 h. We proved in Fig. S6 and Fig. S7 that the GPR models can help in understanding the non-trivial heating rate effect. We can incorporate in Fig. 7 the abstracted knowledge contained in $GPR_{T_{gel}}$ about the heating rate effect on the rheology of MC. In other words, it is possible to predict experimental DMTA curves at given heating rates and frequencies by exploiting $GPR_{T_{gel}}$ and $GPR_{G',G''}$. The reader can find more about this in the Supplementary Information; there we predicted the DMTA curve for a system with c of 1.5 wt.%, tested at different conditions.

Observing the effect of ω on the hysteresis shapes in Fig. 7a–o, we can observe that the loop in $G''(T)$ changed significantly depending on the magnitude of ω. At low frequencies $G''(T)$ approximated to the shape of $G'(T)$ and as ω increased, $G''(T)$ transitions to a butterfly shape. In fact, at the highest c level and ω, the hysteresis reduced drastically, meaning that the sol-to-gel and gel-to-sol transitions in MC could follow a similar mechanism.

Remarkably, the appearance of a butterfly-shaped hysteresis loop in $G''(T)$ at $\omega \geq 10$ rad s^{-1} indicated a change in the gel structure. We can also observe that the initial magnitude of $G'(T)$ increased as ω increased. This behavior is typical in polymers; a high frequency reduces the timespan for the polymer to relax, incrementing the magnitude of the storage and loss modulus. To the best of our knowledge, this is the first time the effects of ω, T, and c on the material properties of MC have been studied comprehensively. Thanks to the aid of ML, we can visualize the timescale effect on the thermogelation process of MC. We believe that the relationship between ω, T, and c will supplement future molecular simulations of the percolation phenomenon in MC.

GPR is relevant to studying complex rheological systems, such as MC, where the time–temperature superposition principle is not applicable. Although the surfaces in Fig. S5 could be collapsed into a master curve, as shown in Fig. S8, these master curves require vertical and horizontal shift factors. The vertical shift reduces the physical meaning of the master curve, implying that the short-term behavior of MC does not correspond to that observed at high temperatures and vice versa. As we hypothesized, GPR allowed us to explain the rheological behavior of MC as a function of time and temperature in the absence of a master curve. The frequency-dependent rheological behavior reflected the interplay between the timescales of gelation processes, providing insights into how the material transitions from a liquid to a gel state under different conditions. At lower frequencies, where the timescales are longer, the system has more time for molecular rearrangements and the establishment of the gel network. This prolonged timescale favors the development of a more viscous response, allowing the polymer chains to entangle and form the gel structure over time. Conversely, at

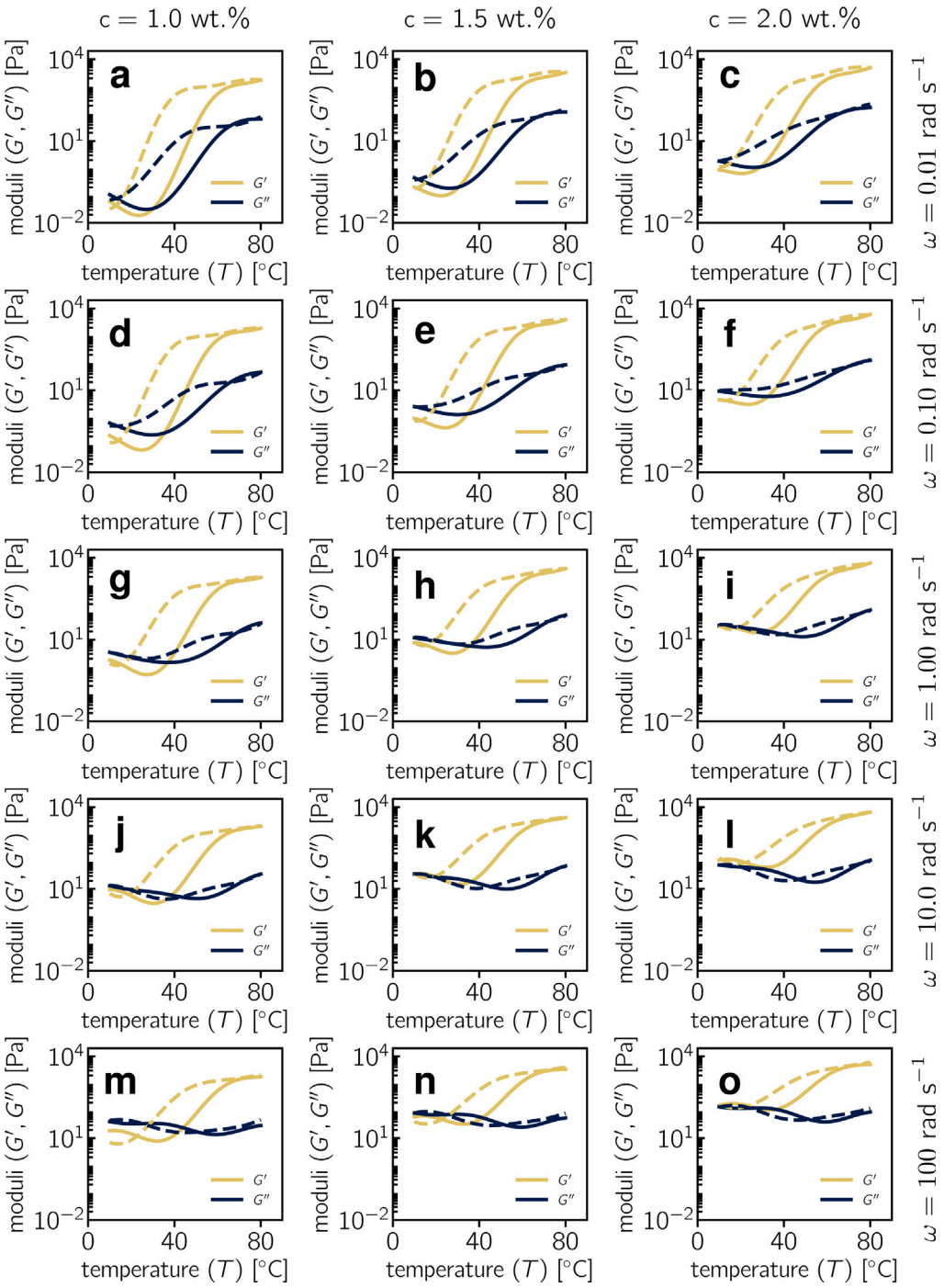

Fig. 7. Machine Learning-constructed rheograms showing the thermal hysteresis in the storage G' and loss modulus G'' at multiple angular frequencies (ω) and varying the polymer concentration (c) in the MC systems. a–o Each rheogram shows G' and G'' during heating (solid lines) and cooling (dashed lines). The corresponding c and ω for a rheogram are given by the label on the uppermost and right side of the figure.

higher frequencies, the timescale becomes shorter, limiting the material to undergo extensive molecular rearrangements. This results in a more elastic response due to reduced molecular mobility.

We finally computed T_{gel} of MC based on ω and c using the data extracted from $\mathrm{GPR}_{G',G''}$. This was achieved by calculating the phase shift angle δ as $\arctan(G''/G')$, as seen in Fig. S9a. The results of T_{gel} in Fig. S9b follow a similar trend to the one shown in Fig. 5c. In other words, increasing ω (which reduces the time window between oscillations) delayed T_{gel} up to 10 °C in the systems with the lowest c. In Fig. S9c, we also computed the "anti-gelation" temperature (gel-to-sol) and observed that this temperature could be independent of ω. However, there is no standard procedure for determining the gel-to-sol temperature from DMTA data. Therefore, we recommend that future works assess the representative point to characterize the inverse process from DMTA.

4. Conclusion

We have demonstrated the potential of Gaussian Process Regression in rheology by analyzing the thermogelation phenomenon in aqueous methylcellulose structured fluids. Using Active Learning with GPR as a surrogate function, the machine learning approach allowed us to

successfully map the gelation temperature of MC in connection to two important parameters in dynamic mechanical thermal analysis: heating rate and MC concentration. A challenge the AL with GPR overcomes is the typical need for large datasets for training machine learning models. The latter is possible because our framework incorporates prior knowledge (here, the choice of a Gaussian Process with constant mean and the RBF kernel) into the machine learning process. This enables the probing of high-dimensional search spaces with a relatively minor number of data points. The use of AL and GPR has potential applications in Bayesian Optimization workflows. For instance, the approach used in this paper has also been used to optimize compositions of polymers and alloys [6,49]. A future direction for our research would be to implement multi-objective decision-making algorithms in the AL workflow. The latter would allow us to explore and exploit high-dimensional spaces while looking to optimize more than one material property.

We have also shown that GPR alone can help to abstract rheological data into knowledge. In particular, GPR is particularly useful for analyzing complex materials like methylcellulose. This material does not conform to the time–temperature superposition principle, making traditional phenomenological modeling insufficient to describe the system. Our approach has shown that a GPR model can be trained with frequency sweep results. In the absence of time–temperature superposition for MC, with the GPR model, we constructed hysteresis plots that characterize $G'(T)$ and $G''(T)$ at a range of angular frequencies that cannot be measured physically or would require experiments to last days. Besides providing a comprehensive understanding of the impact of ω, T, and c on the material properties of MC, our study explores a machine learning method with significant potential in soft matter science. The GPR approach could be utilized in the future to develop self-driven laboratories and high-throughput rheometers aimed at optimizing and discovering new materials.

CRediT authorship contribution statement

Marie Sourroubille: Methodology, Investigation. **Isaac Y. Miranda-Valdez:** Writing – review & editing, Writing – original draft, Visualization, Software, Methodology, Investigation, Formal analysis, Conceptualization. **Tero Mäkinen:** Writing – review & editing, Validation. **Juha Koivisto:** Writing – review & editing, Validation, Supervision, Funding acquisition. **Mikko J. Alava:** Writing – review & editing, Validation, Supervision, Project administration, Funding acquisition.

Declaration of competing interest

The authors declare that they have no known competing financial interests or personal relationships that could have appeared to influence the work reported in this paper.

Acknowledgments

I.M-V. thanks funding from the Vilho, Yrjö and Kalle Väisälä Foundation of the Finnish Academy of Science and Letters. M.J.A. and J.K. thank FinnCERES flagship (151830423), Business Finland (211835), and Future Makers programs. M.J.A., T.M., and I.M-V. thank Business Finland (211909). The authors thank the Aalto University School of Science "Science-IT" project for the computational resources provided. I.M-V. thanks Prof. Valeriy Ginzburg for his helpful discussion about the master curve of methylcellulose.

Appendix A. Supplementary data

Supplementary materials are available.

Supplementary material related to this article can be found online at https://doi.org/10.1016/j.colsurfa.2024.136057.

Data availability

Data will be made available on request.

References

[1] K.T. Butler, D.W. Davies, H. Cartwright, O. Isayev, A. Walsh, Machine learning for molecular and materials science, Nature 559 (7715) (2018) 547–555, http://dx.doi.org/10.1038/s41586-018-0337-2.

[2] P.S. Clegg, Characterising soft matter using machine learning, Soft Matter 17 (15) (2021) 3991–4005, http://dx.doi.org/10.1039/d0sm01686a.

[3] S.M. Moosavi, B.A. Novotny, D. Ongari, E. Moubarak, M. Asgari, O. Kadioglu, C. Charalambous, A. Ortega-Guerrero, A.H. Farmahini, L. Sarkisov, et al., A data-science approach to predict the heat capacity of nanoporous materials, Nature Mater. 21 (12) (2022) 1419–1425, http://dx.doi.org/10.1038/s41563-022-01374-3.

[4] K.R. Lennon, G.H. Mckinley, J.W. Swan, A data-driven method for automated data superposition with applications in soft matter science, Data-Centric Eng. 4 (2023) e13, http://dx.doi.org/10.1017/dce.2023.3.

[5] E. Yang, J.F. Pressly, B. Natarajan, R. Colby, K.I. Winey, R.A. Riggleman, Understanding creep suppression mechanisms in polymer nanocomposites through machine learning, Soft Matter 19 (39) (2023) 7580–7590, http://dx.doi.org/10.1039/d3sm00898c.

[6] V. Torsti, T. Mäkinen, S. Bonfanti, J. Koivisto, M.J. Alava, Improving the mechanical properties of cantor-like alloys with Bayesian optimization, APL Mach. Learn. 2 (1) (2024) (in press).

[7] T. Xie, J.C. Grossman, Crystal graph convolutional neural networks for an accurate and interpretable prediction of material properties, Phys. Rev. Lett. 120 (14) (2018) 145301, http://dx.doi.org/10.1103/physrevlett.120.145301.

[8] W. Ye, C. Chen, Z. Wang, I.-H. Chu, S.P. Ong, Deep neural networks for accurate predictions of crystal stability, Nature Commun. 9 (1) (2018) 3800, http://dx.doi.org/10.1038/s41467-018-06322-x.

[9] A.R. Dulaney, J.F. Brady, Machine learning for phase behavior in active matter systems, Soft Matter 17 (28) (2021) 6808–6816, http://dx.doi.org/10.1039/d1sm00266j.

[10] M.P. Lourenço, A. Tchagang, K. Shankar, V. Thangadurai, D.R. Salahub, Active learning for optimum experimental design—insight into perovskite oxides, Can. J. Chem. 101 (9) (2023) 734–744, http://dx.doi.org/10.1139/cjc-2022-0198.

[11] T. Lookman, P.V. Balachandran, D. Xue, R. Yuan, Active learning in materials science with emphasis on adaptive sampling using uncertainties for targeted design, npj Comput. Mater. 5 (1) (2019) 21, http://dx.doi.org/10.1038/s41524-019-0153-8.

[12] S. Greenhill, S. Rana, S. Gupta, P. Vellanki, S. Venkatesh, Bayesian optimization for adaptive experimental design: A review, IEEE Access 8 (2020) 13937–13948, http://dx.doi.org/10.1109/access.2020.2966228.

[13] D. Khatamsaz, B. Vela, P. Singh, D.D. Johnson, D. Allaire, R. Arróyave, Bayesian optimization with active learning of design constraints using an entropy-based approach, npj Comput. Mater. 9 (1) (2023) 49, http://dx.doi.org/10.1038/s41524-023-01006-7.

[14] J. Löfgren, D. Tarasov, T. Koitto, P. Rinke, M. Balakshin, M. Todorović, Machine learning optimization of lignin properties in green biorefineries, ACS Sustain. Chem. Eng. 10 (29) (2022) 9469–9479, http://dx.doi.org/10.1021/acssuschemeng.2c01895.

[15] L. Bassman Oftelie, P. Rajak, R.K. Kalia, A. Nakano, F. Sha, J. Sun, D.J. Singh, M. Aykol, P. Huck, K. Persson, P. Vashishta, Active learning for accelerated design of layered materials, npj Comput. Mater. 4 (1) (2018) 74, http://dx.doi.org/10.1038/s41524-018-0129-0.

[16] R. Pollice, G. Dos Passos Gomes, M. Aldeghi, R.J. Hickman, M. Krenn, C. Lavigne, M. Lindner-D'Addario, A. Nigam, C.T. Ser, Z. Yao, et al., Data-driven strategies for accelerated materials design, Acc. Chem. Res. 54 (4) (2021) 849–860, http://dx.doi.org/10.1021/acs.accounts.0c00785.

[17] S. Diwale, M.K. Eisner, C. Carpenter, W. Sun, G.C. Rutledge, R.D. Braatz, Bayesian optimization for material discovery processes with noise, Mol. Syst. Des. Eng. 7 (6) (2022) 622–636, http://dx.doi.org/10.1039/d1me00154j.

[18] A.G. Kusne, H. Yu, C. Wu, H. Zhang, J. Hattrick-Simpers, B. Decost, S. Sarker, C. Oses, C. Toher, S. Curtarolo, A.V. Davydov, R. Agarwal, L.A. Bendersky, M. Li, A. Mehta, I. Takeuchi, On-the-fly closed-loop materials discovery via Bayesian active learning, Nature Commun. 11 (1) (2020) 5966, http://dx.doi.org/10.1038/s41467-020-19597-w.

[19] I.Y. Miranda-Valdez, L. Viitanen, J. Mac Intyre, A. Puisto, J. Koivisto, M. Alava, Predicting effect of fibers on thermal gelation of methylcellulose using Bayesian optimization, Carbohydr. Polymers 298 (2022) 119921, http://dx.doi.org/10.1016/j.carbpol.2022.119921.

[20] M. Ziatdinov, Y. Liu, K. Kelley, R. Vasudevan, S.V. Kalinin, Bayesian active learning for scanning probe microscopy: From Gaussian processes to hypothesis learning, ACS Nano 16 (9) (2022) 13492–13512, http://dx.doi.org/10.1021/acsnano.2c05303.

[21] J.K. Pedersen, C.M. Clausen, O.A. Krysiak, B. Xiao, T.A.A. Batchelor, T. Löffler, V.A. Mints, L. Banko, M. Arenz, A. Savan, et al., Bayesian optimization of high-entropy alloy compositions for electrocatalytic oxygen reduction**, Angew. Chem. Int. Ed. Engl. 60 (45) (2021) 24144–24152, http://dx.doi.org/10.1002/anie.202108116.

[22] P.S. Ramesh, T.K. Patra, Polymer sequence design via molecular simulation-based active learning, Soft Matter 19 (2) (2023) 282–294, http://dx.doi.org/10.1039/d2sm01193j.

[23] M. Reichler, S. Rabensteiner, L. Törnblom, S. Coffeng, L. Viitanen, L. Jannuzzi, T. Mäkinen, J.R. Mac Intyre, J. Koivisto, A. Puisto, et al., Scalable method for bio-based solid foams that mimic wood, Sci. Rep. 11 (1) (2021) 24306, http://dx.doi.org/10.1038/s41598-021-03764-0.

[24] I.Y. Miranda-Valdez, J. Puente-Córdova, F. Rentería-Baltiérrez, L. Fliri, M. Hummel, A. Puisto, J. Koivisto, M. Alava, Viscoelastic phenomena in methylcellulose aqueous systems: Application of fractional calculus, Food Hydrocolloids (2023) http://dx.doi.org/10.1016/j.foodhyd.2023.109334.

[25] I.Y. Miranda-Valdez, S. Coffeng, Y. Zhou, L. Viitanen, X. Hu, L. Jannuzzi, A. Puisto, M.A. Kostiainen, T. Mäkinen, J. Koivisto, et al., Foam-formed biocomposites based on cellulose products and lignin, Cellulose 30 (4) (2023) 2253–2266, http://dx.doi.org/10.1007/s10570-022-05041-3.

[26] I.Y. Miranda-Valdez, M.R. Yazdani, T. Mäkinen, S. Coffeng, L. Viitanen, J. Koivisto, M.J. Alava, Cellulose foams as scalable templates for phase change materials, J. Energy Storage 73 (2023) 109036, http://dx.doi.org/10.1016/j.est.2023.109036.

[27] H. Jeong, J. Lee, Y.-J. Jo, M.-J. Choi, Thermo-irreversible emulsion gels based on deacetylated konjac glucomannan and methylcellulose as animal fat analogs, Food Hydrocolloids 137 (2023) 108407, http://dx.doi.org/10.1016/j.foodhyd.2022.108407.

[28] A. Andrade, S. Henríquez-Gallegos, G. Albornoz-Palma, M. Pereira, Effect of the chemical and structural characteristics of pulps of Eucalyptus and Pinus on the deconstruction of the cell wall during the production of cellulose nanofibrils, Cellulose 28 (9) (2021) 5387–5399, http://dx.doi.org/10.1007/s10570-021-03848-0.

[29] K.A. Henn, N. Forsman, T. Zou, M. Österberg, Colloidal lignin particles and epoxies for bio-based, durable, and multiresistant nanostructured coatings, ACS Appl. Mater. Interfaces 13 (29) (2021) 34793–34806, http://dx.doi.org/10.1021/acsami.1c06087.

[30] L. Viitanen, I.Y. Miranda-Valdez, J. Koivisto, A. Puisto, M. Alava, Thermal gelation of cellulose based suspensions, Cellulose 30 (7) (2023) 4215–4223, http://dx.doi.org/10.1007/s10570-023-05150-7.

[31] F. Pedregosa, G. Varoquaux, A. Gramfort, V. Michel, B. Thirion, O. Grisel, M. Blondel, P. Prettenhofer, R. Weiss, V. Dubourg, J. Vanderplas, A. Passos, D. Cournapeau, M. Brucher, M. Perrot, E. Duchesnay, Scikit-learn: Machine learning in python, J. Mach. Learn. Res. 12 (2011) 2825–2830.

[32] M.L. Coughlin, L. Liberman, S.P. Ertem, J. Edmund, F.S. Bates, T.P. Lodge, Methyl cellulose solutions and gels: Fibril formation and gelation properties, Prog. Polym. Sci. 112 (2021) 101324, http://dx.doi.org/10.1016/j.progpolymsci.2020.101324.

[33] L. Barbier, M. Protat, P. Pipart, A. Marcellan, Y. Tran, D. Hourdet, Sol/gel transition of thermoresponsive Hyaluronan: From liquids to elastic and sticky materials, Carbohydr. Polymers 310 (2023) 120715, http://dx.doi.org/10.1016/j.carbpol.2023.120715.

[34] J. Desbrières, M. Hirrien, S. Ross-Murphy, Thermogelation of methylcellulose: Rheological considerations, Polymer 41 (7) (2000) 2451–2461, http://dx.doi.org/10.1016/S0032-3861(99)00413-9.

[35] J.R. Lott, J.W. Mcallister, S.A. Arvidson, F.S. Bates, T.P. Lodge, Fibrillar structure of methylcellulose hydrogels, Biomacromolecules 14 (8) (2013) 2484–2488, http://dx.doi.org/10.1021/bm400694r.

[36] P.W. Schmidt, S. Morozova, S.P. Ertem, M.L. Coughlin, I. Davidovich, Y. Talmon, T.M. Reineke, F.S. Bates, T.P. Lodge, Internal structure of methylcellulose fibrils, Macromolecules 53 (1) (2020) 398–405, http://dx.doi.org/10.1021/acs.macromol.9b01773.

[37] V.V. Ginzburg, R.L. Sammler, W. Huang, R.G. Larson, Anisotropic self-assembly and gelation in aqueous methylcellulose—theory and modeling, J. Polym. Sci. B 54 (16) (2016) 1624–1636, http://dx.doi.org/10.1002/polb.24065.

[38] S.A. Arvidson, J.R. Lott, J.W. Mcallister, J. Zhang, F.S. Bates, T.P. Lodge, R.L. Sammler, Y. Li, M. Brackhagen, Interplay of phase separation and thermoreversible gelation in aqueous methylcellulose solutions, Macromolecules 46 (1) (2013) 300–309, http://dx.doi.org/10.1021/ma3019359.

[39] J.W. Mcallister, P.W. Schmidt, K.D. Dorfman, T.P. Lodge, F.S. Bates, Thermodynamics of aqueous methylcellulose solutions, Macromolecules 48 (19) (2015) 7205–7215, http://dx.doi.org/10.1021/acs.macromol.5b01544.

[40] C. Alamprese, M. Mariotti, Modelling of methylcellulose thermogelation as a function of polymer concentration and dissolution media properties, LWT - Food Sci. Technol. 60 (2, Part 1) (2015) 811–816, http://dx.doi.org/10.1016/j.lwt.2014.10.067.

[41] N. Bizmark, N.J. Caggiano, J.X. Liu, C.B. Arnold, R.K. Prud'Homme, S.S. Datta, R.D. Priestley, Hysteresis in the thermally induced phase transition of cellulose ethers, Soft Matter 18 (33) (2022) 6254–6263, http://dx.doi.org/10.1039/d2sm00564f.

[42] F. Ziembowicz, D.V. de Freitas, C.R. Bender, P.R. dos Santos Salbego, C. Piccinin Frizzo, M.A. Pinto Martins, J.M. Reichert, I.T. Santos Garcia, C.L. Kloster, M.A. Villetti, Effect of mono- and dicationic ionic liquids on the viscosity and thermogelation of methylcellulose in the semi-diluted regime, Carbohydr. Polymers 214 (2019) 174–185, http://dx.doi.org/10.1016/j.carbpol.2019.02.095.

[43] T. Sanz, A. Salvador, S. Fiszman, Effect of concentration and temperature on properties of methylcellulose-added batters application to battered, fried seafood, Food Hydrocolloids 18 (1) (2004) 127–131, http://dx.doi.org/10.1016/S0268-005X(03)00050-X.

[44] W. Sun, A.P. Vassilopoulos, T. Keller, Effect of thermal lag on glass transition temperature of polymers measured by DMA, Int. J. Adhes. Adhes. 52 (2014) 31–39, http://dx.doi.org/10.1016/j.ijadhadh.2014.03.009.

[45] R.H. Ebini, C.M. Sorensen, Light scattering studies of the sol-to-gel transition in particulate systems, J. Colloid Interface Sci. 556 (2019) 577–583, http://dx.doi.org/10.1016/j.jcis.2019.08.075.

[46] T. Hjelt, J.A. Ketoja, H. Kiiskinen, A.I. Koponen, E. Pääkkönen, Foam forming of fiber products: A review, J. Dispers. Sci. Technol. 43 (10) (2022) 1462–1497, http://dx.doi.org/10.1080/01932691.2020.1869035.

[47] K. Mobredi, I.Y. Miranda-Valdez, T. Mäkinen, J. Koivisto, M.J. Alava, A simple approach to produce hydrophobic biobased coatings using methylcellulose and organosolv lignin, Soft Matter 20 (28) (2024) 5607–5615.

[48] I.Y. Miranda-Valdez, T. Mäkinen, X. Hu, J. Lejon, M. Elamir, L. Viitanen, L. Jannuzzi, J. Koivisto, M.J. Alava, Bio-based foams to function as future plastic substitutes by biomimicry: Inducing hydrophobicity with lignin, Adv. Eng. Mater. 26 (20) (2024) 2400233.

[49] I.Y. Miranda-Valdez, T. Mäkinen, S. Coffeng, A. Päivänsalo, L. Jannuzzi, L. Viitanen, J. Koivisto, M.J. Alava, Accelerated design of solid bio-based foams for plastics substitutes, Mater. Horiz. (2025) http://dx.doi.org/10.1039/d4mh01464b, Advance Article.